of today, however, and the global climate may then have been much more sensitive to solar variability than is now observed[3].

The Elatina record, in view of its clarity and great length, accordingly may provide invaluable data on which to model the physics of the solar activity cycle[3,17]. The implications of these new data for solar physics and planetary science will be addressed separately.

G.E.W. thanks the Trustees of the CSIRO Science and Industry Endowment Fund for sponsoring the diamond drilling of the Elatina Formation; Dr W. Robinson, Director, Laboratory of Tree-Ring Research, University of Arizona, for a temporary appointment and valuable assistance; and the National Solar Observatory, Tucson, for a visiting scientist appointment. Helpful discussions on various aspects of the work were held with Drs L. Cram, R. Loughhead, C. Durrant, W. Livingston, J. Goad, R. Jokipii, A. Skumanich, R. Bracewell, N. Alley and C. Farrelly. T. Trebisky was responsible for much of the programming. The research was in part supported by the NSF.

Received 23 May; accepted 26 September 1985.

1. Williams, G. E. *Nature* **291**, 624–628 (1981).
2. Williams, G. E. in *Weather and Climate Responses to Solar Variations* (ed. McCormac, B. M.) 517–533 (Colorado Associated University Press, Boulder, 1983).
3. Williams, G. E. *Aust. J. Phys.* (in the press).
4. Williams, G. E. & Tonkin, D. G. *Aust. J. Earth Sci.* (in the press).
5. Smith, N. D. *Can. J. Earth Sci.* **15**, 741–756 (1978).
6. Perkins, J. A. & Sims, J. D. *Quat. Res.* **20**, 308–321 (1983).
7. Cohen, T. J. & Lintz, P. R. *Nature* **250**, 398–400 (1974).
8. Herman, J. R. & Goldberg, R. A. *Sun, Weather, and Climate* (NASA, Washington DC, 1978).
9. Sonett, C. P. *Geophys. Res. Lett.* **9**, 1313–1316 (1982).
10. Sonett, C. P. *Rev. Geophys. Space Phys.* **22**, 239–254 (1984).
11. Sonett, C. P. & Suess, H. E. *Nature* **307**, 141–143 (1984).
12. Mörner, N.-A. in *Climatic Changes on a Yearly to Millennial Basis* (eds Mörner, N.-A. & Karlén, W.) 1–13 (Reidel, Dordrecht, 1984).
13. Treut, H. Le & Ghil, M. *J. geophys. Res.* **88**, 5167–5190 (1983).
14. Waldmeier, M. *The Sunspot-Activity in the Years 1610–1960* (Schulthess, Zürich, 1961).
15. Howard, R., Gilman, P. A. & Gilman, P. E. *Astrophys. J.* **283**, 373–384 (1984).
16. Wilson, R. M. *NASA tech. Paper* **2325** (1984).
17. Bracewell, R. N. *Aust. J. Phys.* (in the press).
18. Sonett, C. P. & Williams, G. E. *J. geophys. Res.* (in the press).
19. Cloud, P. *Geol. Soc. Am. Mem.* **161**, 245–251 (1983).

Thermally induced residual topography within oceanic lithosphere

Garry D. Karner

Department of Geological Sciences, University of Durham, Durham DH1 3LE, UK

The lithosphere, following a thermal event, should subside isostatically to its pre-event configuration. However, if the thermal event is sufficient to reset the rigidity of the lithosphere, then the subsidence is forced to follow a different path to the initial uplift; lithospheric rigidity decrease during uplift allows flexural deformation resetting, while during subsidence, an increasing rigidity with time results in flexural interference. This 'thermo-mechanical hysteresis' effect may be responsible for anomalous bathymetry and free-air gravity anomalies associated with hotspot traces, extinct spreading centres and the ocean/continent boundary of rifted (passive continental) margins.

BROAD-SCALE reheating of the lithosphere is the result of thermal processes such as hotspot volcanism, rifting and possibly small-scale mantle convection. Concomitant with thermal modification of the lithosphere is its isostatic uplift and mechanical weakening (rigidity decrease). The actual uplift topography is a function of only the minimum rigidity obtained during heating. Subsequent cooling of the lithosphere allows its subsidence and mechanical recovery (increasing flexural rigidity with time). However, in marked contrast to the uplift, the cumulative subsidence is a function of the entire mechanical recovery history of the lithosphere. Flexural interference between this cumulative uplift and the initial topography produces a residual topography, the amplitude and wavelength of which critically depends on the rate of mechanical recovery and the degree of lithospheric heating.

The production of residual topography, as it involves the entire crust, resembles a buckled elastic plate. Even though such topography will necessarily be associated with large free-air gravity anomalies, the forces responsible for the deformation remain in mechanical and isostatic equilibrium at all times as evidenced by the equal positive and negative components of both the topography and free-air gravity anomaly. Formation of residual topography by the flexural interference of thermally modified lithosphere is here termed 'thermo-mechanical hysteresis' (TMH). It is suggested that TMH may be responsible for the characteristic free-air gravity anomalies observed over extinct spreading centres, for example, within the South China Sea and the Coral Sea basins, the isostatic gravity anomaly observed across the ocean/continent boundary of many passive margins, for example Argentina and the northeastern US margins, and anomalous bathymetric trends within the major oceanic plates, for example, the linear bathymetric trend associated with the Cocos–Keeling Islands in the Indian Ocean.

Structure of the lithosphere

The interdependence of the thermal structure of the lithosphere and its mechanical properties has been convincingly demonstrated by recent studies of loading within the oceans and continents[1–5]. Furthermore, these studies have established that flexure is the predominant mechanism by which emplaced loads are supported by the lithosphere. The form of the support is dependent on the lithospheric rigidity, which itself increases with lithospheric age. Generally, in the oceans, the plate age defines the thermal structure of the lithosphere through the cooling plate model[6], while in the continents, rather than absolute plate age being important, it is the time since the last major thermal event as defined by either reset radiometric basement ages[1] or episodes of extensive alkalic or basic volcanism[7].

Observations of the subsidence of seamounts associated with intraplate swells suggest that the swells behave like oceanic crust reset to a younger thermal age[2,8–11]. The swells, in turn, are related to the broad-scale heating and hence thermal expansion of the lithosphere above hotspots (for example, Hawaii, Snake River province) or hot-lines (for example, Easter Island chain[12], eastern Australia[13,14]).Thermal rejuvenation results in a lithosphere with properties identical to that of normal lithosphere but with an apparent younger thermal age and correspondingly lower lithospheric rigidity[2].

Thermal modification of the lithosphere by a general heating event causes an immediate isostatic uplift in an attempt to compensate the thermally expanded lower lithosphere[15,16]. Isostatic compensation is essentially supplied by a Pratt-type pro-

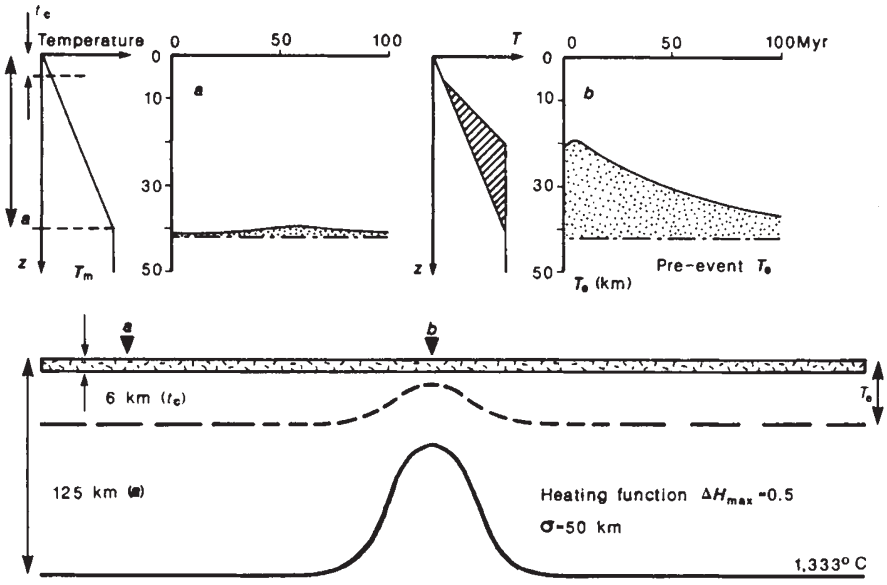

Fig. 1 Schematic representation of the initial rigidity structure of the lithosphere, the distribution of the heating function (parametrized by ΔH_{max} and σ), the initial thermal structure over the zone of maximum heating and in the distant regions of the plate, and the mechanical recovery of the lithosphere (that is, the variation of T_e, the effective elastic thickness of the lithosphere) with time.

cess in which the uplifted topography compensates the lower densities associated with the thermally modified lithosphere. Even though Pratt isostasy is a local compensation scheme, the form and maximum amplitude of the surface deformation will be determined by the minimum lithospheric rigidity obtained during the thermal resetting process (in both space and time). Because plate rigidity is defined by the depth to a particular isotherm (in this case, the 450 °C isotherm[5]), minimum rigidity resetting occurs some time after the initiation of cooling as heat is removed vertically from the lower lithosphere to the upper lithosphere (Fig. 1). Second, minor heating associated with lateral heat flow eventually modifies rigidities in the distant regions of the plate. Following the maximum deformation stage, cooling of the lithosphere by vertical and lateral heat flow will result in a spatially and temporally varying flexural rigidity. In particular, the temporally increasing flexual rigidity will produce a progressively broader subsidence with time relative to the initial uplift. Flexural interference between this initial uplift and subsequent broader subsidence results in a residual topography. The purpose of this article therefore, is to model quantitatively the thermo-mechanical response of the lithosphere due to thermal loading and to define the production and form of residual topography.

Thermal loading

Several studies have suggested that mid-plate swells are adequately approximated by a gaussian-type heating function[10]. For convenience, the same functional form will be assumed for the distribution of the thermal load in this study. Heat input into the lithosphere can be characterized by the dimensionless quantity[16] ΔH, where $\Delta H = 1$ represents complete melting of the lithosphere while $\Delta H = 0$ represents stable thermal equilibrium within the lithosphere. The degree of lithospheric heating can also be expressed in terms of the lithospheric stretching function of McKenzie[15], and, in particular, the two-layer stretching model of Royden and Keen[16], even though no literal stretching is implied. In particular,

$$\Delta H = (1 - 1/\beta)\left(\frac{a - t_c}{a}\right)^2 \exp\left[-x^2/\sigma^2\right]$$

$$\Delta H_{max} = 0.5, \qquad \beta_{max} = 2.5$$

where ΔH_{max} is the maximal thermal heating, β is typically the stretching of the sub-crustal lithosphere, σ is the half-width of the heating function (with modelling constants defined in Table 1), a is the lithospheric thickness, t_c the oceanic crustal thickness and x is the horizontal coordinate. As the lithosphere/asthenosphere boundary represents an isotherm (T_m), β can define not only the degree of sub-crustal stretching, but also the maximum vertical migration of this temperature boundary and therefore the degree of subcrustal heating. The use of β does not necessarily imply a tectonic process or setting. However, the actual details of the heating process or the distribution of the thermal anomaly itself are not critical to this argument. Whenever a load, thermal or otherwise, is removed incrementally from the lithosphere while the flexural rigidity is varied, a permanent lithospheric deformation results. This article links the thermal loading (and subsequent unloading as the load is conductively dissipated) of the lithosphere with its thermal and hence mechanical modification (and subsequent recovery). By calculating $\beta(x)$ from ΔH, the initial (or instantaneous) surface uplift is[17],

$$S_i = \frac{\alpha \rho_m T_m}{2(\rho'_m - \rho_w)} \Delta H(x)$$

where α is the thermal expansion coefficient, and ρ_m, ρ'_m and ρ_w are the mantle density at 0 °C, the asthenosphere density and the water density, respectively.

The initial surface uplift S_i, assumes that the lithosphere has zero flexural strength (Pratt or local isostasy) and is termed the

Table 1 Modelling parameters used

Parameter value	Definition
$a = 125$ km	Lithospheric thickness
$t_c = 6$ km	Oceanic crustal thickness
$\kappa = 0.008$ cm^2 s^{-2}	Thermal diffusivity
$\alpha = 3.4 \times 10^{-5}$ °C^{-1}	Thermal expansion coefficient
$T_m = 1{,}333$ °C	Temperature defining lithosphere
$\tau = 62.8$ Myr	Thermal relaxation coefficient
$Z_e = 450$ °C	Controlling elastic isotherm
$\rho_w = 1.03$ g cm^{-3}	Water density } ρ_i
$\rho_s = 2.5$	Sediment density }
$\rho_m = 3.33$	Mantle density at 0 °C
$\rho'_m = \rho_m(1 - \alpha T_m) = 3.179$	Asthenosphere density
$g = 982$ cm s^{-2}	Acceleration due to gravity
$\gamma = 6.673 \times 10^{-8}$ cm^3 g^{-2} s^{-2}	Gravitational constant
$\Delta H_{max} = 0.5$	Maximum thermal heating
$\beta_{max} = 2.5$	Equivalent sub-crustal stretching value
$\sigma = 50$ km	Standard deviation of heating function
$D = ET_e^3/12(1 - \nu^2)$	Lithospheric rigidity
T_e	Effective elastic thickness
$E = 6.5 \times 10^{11}$ dyn cm^{-2}	Relaxed Young's modulus
$\nu = 0.25$	Poisson's ratio

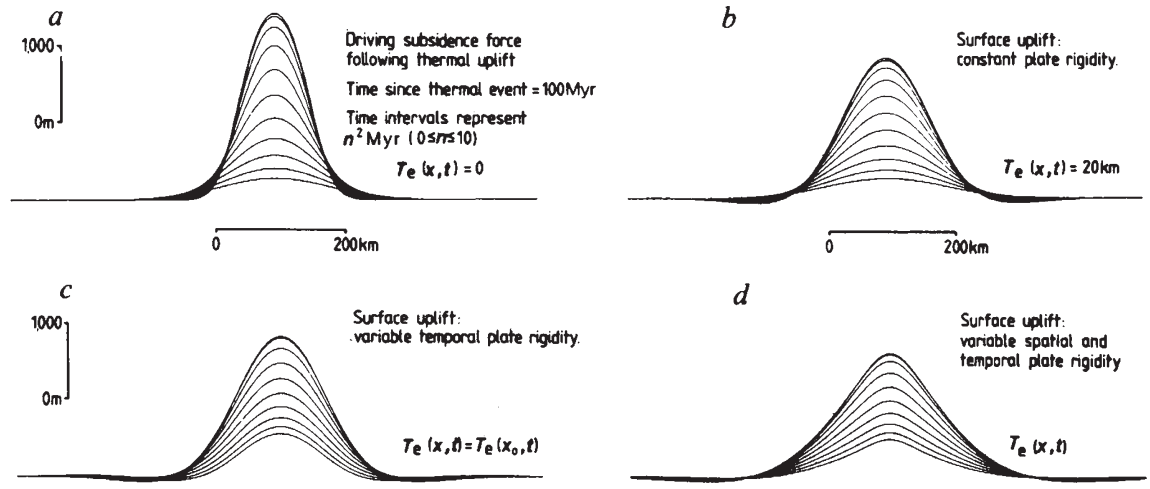

Fig. 2 Following a thermal event, the driving subsidence associated with the cooling and contraction of the lithosphere opposes the initial uplift, itself associated with a thermal buoyancy force. The resulting time-dependent force balance is subsequently modified by the mechanical properties of the lithosphere, producing a time-varying surface topography. The surface topography is illustrated for various assumptions of the mechanical response of the lithosphere at 0, 4, 9, 16, 25, 49, 64, 81 and 100 Myr since the initiation of cooling. Modelling parameters are defined in Table 1. *a*, Surface response of the lithosphere assuming a local isostatic response to loading. As local compensation refers to a zero-rigidity lithosphere, the form of the surface response is equivalent to the resultant force acting on the lithosphere. As lithospheric cooling has been modelled using both vertical and lateral heat flow, the force spreads laterally with time. *b*, Surface response of the lithosphere assuming a constant rigidity. If the thermal event fails to reset the lithospheric rigidity, the uplift and subsidence histories are identical and therefore no residual topography is produced. *c*, Surface response of the lithosphere assuming that its rigidity is reset and subsequently increases with time following the thermal event. The differing uplift and subsidence histories of the lithosphere result in a residual topography, the amplitude and wavelength of which relates to the pre-event rigidity and the degree of resetting. *d*, Surface response of the lithosphere assuming both a spatial and temporal variation in rigidity. The spatial rigidity variations relate to the distribution of the thermal event whereas the temporal variations relate to the thermal properties of the lithosphere. Note that in both *c* and *d* the topographic wavelength decreases with time, implying a progressive decrease in flexural rigidity. Such behaviour is usually interpreted in terms of the flexural response of a (Maxwell) visco-elastic plate to loading. However, in this case, the changing topographic wavelength is simply reflecting the sensitive interrelationship between the mechanical properties of the lithosphere and its temperature structure.

'local uplift'. Although Pratt isostasy (or any local isostatic scheme) generally represents an unrealistic response of the lithosphere to loading, it is very useful in describing the potential uplift of the lithosphere. Convolution of this local uplift with a flexural filter redistributes the surface uplift according to the mechanical properties of the lithosphere. For example, if the lithosphere has constant elastic rigidity D, then the surface uplift is given by (in the frequency domain)[18],

$$S_i^* = \frac{\alpha\rho_m T_m}{2(\rho'_m - \rho_w)}\Delta H(k)\left[1 + \frac{Dk^4}{(\rho_m - \rho_i)g}\right]^{-1}$$

where ρ_i is the density of material infilling the deformation, k is the wavenumber, and g is the acceleration due to gravity. As a consequence of thermally modifying the temperature structure of the lithosphere, D is not constant but varies both spatially and temporally in the plate such that $D = D(x, t)$, t being the time since the initiation of lithospheric cooling.

Cooling of the lithosphere by the vertical and lateral flow of heat away from the thermally perturbed zone results in the creation of an opposing subsidence which progressively negates the initial surface uplift. The local subsidence counteracting S_i is given by[19],

$$S_t(x,t) = \frac{2\rho_m\alpha T_m a}{(\rho'_m - \rho_m)} \sum_{n=1}^{\infty\ (n\ \text{odd})} \frac{2}{n^2\pi^2} A_n^*(1 - e^{-n^2 t/\tau})$$

where

$$A_n = \frac{1}{n\pi}\{(1-\beta)\sin(n\pi z_1) + \beta\sin(n\pi z_2)\}$$

$$z_1 = t_c/a, \qquad z_2 = z_1 + (1 - z_1)/\beta$$

$$A_n^* = A_n * X(x,t)$$

$$X(x,t) = \frac{1}{2(\pi\kappa t)^{1/2}}\exp[-x^2/4\kappa t]$$

where $X(x, t)$ represents the lateral conduction of heat, A_n the Fourier series of the initial vertical lithospheric temperature distribution, * the convolution operation, and τ is the thermal relaxation coefficient. As before, the actual subsidence is calculated by convolving $S_t(x, t)$, the local subsidence, with the lateral variations of lithospheric rigidity to give S_t^*. Figure 2*a* summarizes the spatial and temporal behaviour of the local thermal uplift (maximum value of 2,380 m) within the lithosphere for $\Delta H = 0.5$ ($\beta_{max} = 2.5$) and $\sigma = 50$ km (and for times n^2 Myr since initiation of cooling, $1 < n < 10$) and clearly shows the effects of both vertical and lateral heat flow. Because the isostatic compensation in this example is assumed to be local, the uplift is proportional to the thermally generated buoyancy force acting on the lithosphere. With infinite time, the residual local uplift ($S_i - S_t(x, t)$), and therefore the buoyancy force, are identically zero everywhere.

Lithospheric subsidence

Referring to Fig. 2, we can monitor the subsidence of the lithosphere following a thermal event for a variety of mechanical conditions. If we insist on the mechanical homogeneity of the lithosphere both laterally and with time, the residual subsidence ($S_i^* - S_t^*(x, t)$) will again be reduced to zero given sufficient time even with flexural redistribution of the surface uplift (Fig. 2*b*). With $T_e = 20$ km and after 100 Myr, a topographic surface with amplitude 254 m is all that remains from an initial uplift of 1,824 m. If, however, we relax the requirement for temporal homogeneity of the lithospheric rigidity, then the flexural modification of the local subsidence changes continually with time. In this example, the pre-event effective elastic thickness of T_e (42.2 km) is thermally reset to 20 km. Mechanical recovery of the lithosphere over a 100-Myr period increases T_e from 20 to 36.9 km (Fig. 1), producing significant residual topography (431 m, Fig. 2*c*) relative to Fig. 2*b*.

Thermal modification of the lithospheric temperature structure will obviously be greatest nearest the thermal perturbation. Necessarily, therefore, the mechanical properties of the lithosphere must be a function not only of time since the initiation of cooling, but also of the distance from the perturbation. The

redistribution of the local subsidence, $S_i(x, t)$, by a heterogeneous elastic plate to give the flexural subsidence, $S_i^*(x, t)$ is given by,

$$\frac{\partial^2}{\partial x^2}\left[\frac{D(x,t)}{(\rho_m-\rho_i)g}\frac{\partial^2}{\partial x^2}S_i^*(x,t)\right]+S_i^*(x,t)=S_i(x,t)$$

The lateral and temporal variations of plate rigidity, $D(x, t)$, are calculated by monitoring the depth to the 450 °C lithospheric isotherm[5]. The above differential equation is most conveniently solved using a finite-difference algorithm[20]. The resulting topography ($S_i^* - S_i^*(x, t)$) is now the result of a complex interaction between vertical and lateral heat flow and the spatial variations of plate rigidity about the thermal anomaly. Figure 2*d* represents the full model prediction for thermally reset oceanic lithosphere, producing in this example residual topography of 335 m. While the residual topography is only relatively small (100–200 m), note that this deformation was produced with only a modest degree of sub-crustal heating. Areas associated with high-temperature contrasts, such as during the creation of a passive continental margin or during the death of a mid-oceanic spreading centre, will enhance this hysteresis effect and, while probably never dominating, will always be a complicating factor in loading situations when heat is involved.

Apparent visco-elastic behaviour

A curious feature of the residual topography in Fig. 2*c*, *d* is that the wavelength appears to decrease progressively with time implying, therefore, an apparent decrease in flexural rigidity with time even though we are able to monitor its actual increase. That is, the surface deflection is mimicking the temporal response of a visco-elastic (Maxwell) plate. This observation simply underlines the sensitive interrelationship between lithospheric temperature structure and its flexural response and may prove to be useful in rationalizing the apparent contradiction posed by those flexural studies which vehemently refute the elastic model in favour of a visco-elastic (Maxwell) model[21–26].

Apparent visco-elastic behaviour of the lithosphere is not limited to TMH. McNutt[27], in her analysis of seamount flexure, noted that load rejuvenation occurs as the heat introduced into the lithosphere during seamount emplacement is vertically redistributed. The degree of load rejuvenation is therefore sensitive to the level at which the temperature anomaly is introduced. Similarly, foreland basins, produced as an isostatic response to thrust sheet/nappe emplacement[23], modify the temperature structure of the foreland lithosphere (at a rate determined by the thermal diffusivity of the lithosphere) as the overlying sediment infill and thrust sheets thermally re-equilibrate[28]. In both cases, lithospheric heating induces a decrease in rigidity with time which mimics the behaviour of a Maxwell visco-elastic plate.

While thermo-mechanical hysteresis is concerned with load removal during cooling of the lithosphere, a similar flexural interference is obtained during (non-thermal) load emplacement. For example, Liu *et al.*[29] successfully modelled the negative gravity anomaly over the 85° E ridge by investigating the flexural interference between the basement deformation produced by the formation of the ridge and the regional deformation associated with its subsequent burial by sediments. Thermo-mechanical hysteresis, therefore, is only a special case of the flexural interference of lithospheric deformations associated with temporally and/or laterally varying loads and a temporally varying lithospheric rigidity.

Isostatic equilibrium

The isostatic state of the heated lithosphere will be a complicated interaction between the Pratt effect of the thermally modified subcrustal lithosphere and the regional isostatic effect of the evolving crustal deformation. In the limit, however, only the crustal deformation remains. Figure 3 illustrates the residual topography and associated free-air gravity effect produced by thermal re-equilibration of oceanic lithosphere over a 400-Myr period since cooling and for all practical purposes, represents

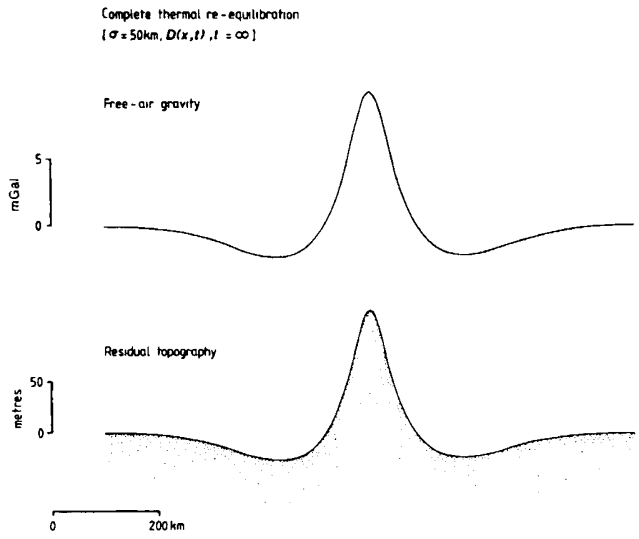

Fig. 3 The resultant free-air gravity effect and residual surface topography following thermal re-equilibration of the lithosphere ($t = 400$ Myr) in which the original thermal perturbation modified both the spatial and temporal flexural properties of the lithosphere. The residual topography and its free-air effect remain an isostatic process in the sense that the topography and free-air gravity laterally integrate to zero (remembering that the Moho parallels the surface).

complete thermal re-equilibrium of the lithosphere. If, during the thermal event, the lithospheric rigidity failed to be reset (that is, remains constant), no residual topography (and hence gravity effect) would be produced. In contrast, any rigidity variation (in space or time) results in a residual topography, in this example being 162 m with a corresponding free-air gravity effect of 20 mGal. Compensation is maintained by the strength of the lithosphere, not in the usual way, but by the production of a surface deformation which laterally integrates to zero (here termed mechanical equilibrium).

Applications

Thermo-mechanical hysteresis results from the thermal re-equilibration of the lithosphere following a heating event. This concept, when applied to the oceanic lithosphere in particular, may help to explain several anomalous bathymetric and gravimetric trends within the Indian Ocean (for example, Cocos-Keeling Islands and associated bathymetric trends), extinct spreading centres (for example, Coral Sea Basin) and ocean/continent boundaries of passive margins (for example, Argentinian margin). No attempt has been made to model the bathymetry or gravity anomalies in detail, but the similarity in characteristics predicted by thermo-mechanical hysteresis, namely, low-amplitude but long-wavelength topography, relatively large-amplitude free-air gravity anomalies relative to the topography (or equivalently, an anomalously high gravitational admittance) and an isostatic compensation reminiscent of mechanical isostasy (a balanced deformation of the entire crust generally reported as uncompensated topography), and the above geological features, strongly suggests that the same process, TMH, may be operative.

Cocos–Keeling hotspot trend

Anomalous north-east–south-west trending bathymetry (1–2 km) within the northern Indian Ocean and generally paralleling the absolute motion of the Indo-Australian plate (Fig. 4*a*) is associated with the Cocos-Keeling Islands, the trend and islands being produced by a presumed hotspot of Lower Tertiary age. Although the bathymetry of the trend is minor relative to the Ninety-East Ridge, the associated free-air gravity anomaly is excessively large (Fig. 4*a*). To remove the effect of the Cocos-

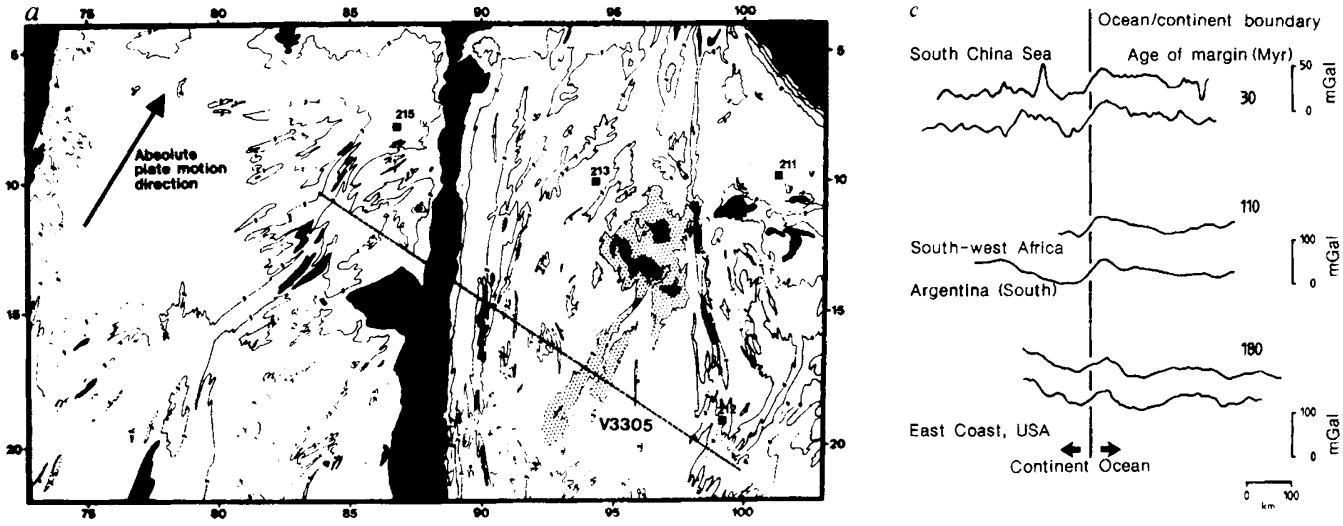

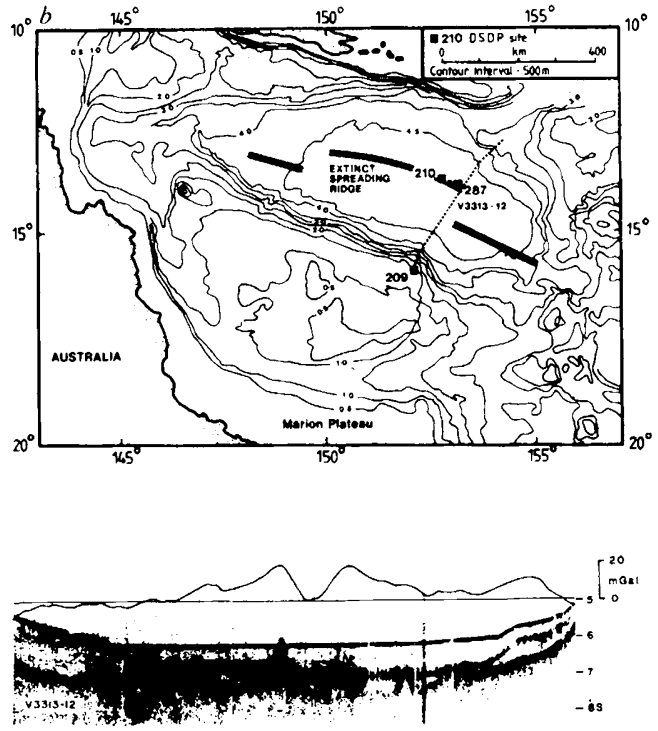

Fig. 4 *a*, Bathymetric contour map of the north-east Indian Ocean. Shading is for depths <4,000 m and highlights the Ninety-East Ridge in particular. Contour intervals are 1,000 m. ■, DSDP sites; dotted line, the ship-track of *Vema* cruise 3305. The anomalous bathymetry associated with the Cocos-Keeling trend is highlighted by the stippled pattern. Profiles of bathymetry, free-air and Bouguer gravity data have been constructed by projecting along-track data perpendicular to the Cocos-Keeling trend. ▲, The trace of possible residual topography which in map form can be seen paralleling the absolute motion of the Indo-Australian plate[41]. The Bouguer density required to remove the topography from the Bouguer anomaly is ~3.2 g cm^{-3}, implying deformation of the entire crust. *b*, Bathymetric map of the Coral Sea Basin, north-east Australia, showing the position of the extinct spreading ridge within the basin as determined from refs 30, 33. Contour intervals are 500 m. Dotted line, the ship-track of *Vema* cruise 3313. Single-channel seismic reflection and free-air gravity anomaly data are shown along this track and illustrate the characteristic free-air gravity anomaly over the extinct spreading centre. Note that the ridge is virtually buried by later sedimentation, thereby significantly reducing the density contrast across the ridge topography. *c*, Isostatic (Airy) gravity profiles across the ocean/continent boundary of passive margins of various ages showing the characteristic dipole form of the anomaly[32,38,39,42]. The ocean/continent boundary represents a major thermal transition between attenuated continental lithosphere and emplaced high-temperature oceanic basalts (as opposed to a passive margin's mechanical transition, the hinge zone of Watts and Steckler[40], which separates highly stretched and unstretched continental lithosphere).

Keeling bathymetry from the observed gravity anomaly requires a Bouguer reduction density of ~3.2 g cm^{-3}, implying that Moho topography is deformed in a similar manner to the surface bathymetry. The association of surface bathymetry with Moho topography implies deformation of the entire crust as required by TMH.

Extinct spreading centres

A second example of thermo-mechanical hysteresis relates to the residual topography associated with extinct spreading centres. While spreading centres represent an inter-plate process, its extinction ensures its incorporation into an intraplate setting. However, its actual tectonic setting is irrelevant; only the long-wavelength ridge topography is supported by a thermal mechanism, collapse of which invokes the thermo-mechanical hysteresis effect. The axial rift valleys of active, slow, spreading centres, such as the Mid-Atlantic Ridge system, are characterized by a short-wavelength (~60 km) free-air gravity low superimposed on a longer-wavelength (~400 km) gravity high. However, this same association of short- and long-wavelength gravity anomalies also exists over extinct spreading centres such as the Coral Sea[30], Labrador Sea[31] and South China Sea basins[32]. This anomaly is so persistent that it has been used to predict the position of extinct spreading axes in the absence of magnetic

anomalies[32,33]. Once spreading has ceased within a rift axis, heat is rapidly dissipated, allowing the ridge topography to subside and thereby destroying its characteristic waveform. In general, the isostatic compensation of spreading ridge topography is poorly understood. Interpretation of admittance functions obtained across active spreading systems[34,35] suggests low lithospheric strengths ($T_e < 10$ km). Seismic studies have shown, however, that oceanic crust is of normal thickness at least to within ~10 m of the ridge axis[36]. As the crustal thickening predicted by isostatic models (in which ridge topography is represented as a surface load) is not observed, such models fail to describe adequately the isostatic state of the ridge. The most promising approach has been to model the ridge topography as the response of a broken elastic plate to a sublithospheric buoyancy force[37], analogous to the thermal event of Fig. 2*a*. The extinction of the spreading ridge system means the eventual dissipation of the thermally generated buoyancy force, ridge subsidence, and as the lithosphere mechanically recovers, the 'freezing-in' of the ridge topography by thermo-mechanical hysteresis.

The extinct spreading centre of the Coral Sea Basin (Fig. 4*b*) is associated with a short-wavelength (~50 km) free-air gravity anomaly low of 15-20 mGal and a longer-wavelength (~350 km) gravity high[30] (Fig. 4*b*). Since the rift valley topography has been buried by turbidites infilling the Coral Sea Basin from Australia and New Guinea, the source of the free-air gravity anomaly is approximately shared between the crust-sediment and crust-mantle interfaces. Calculating the gravity effect of each interface using the Bouguer approximation gives:

Interface (1): 42.2 mGal km^{-1} g^{-1} cm^{-3}

Upward continuation: $\exp(-kd)$; k, the wavenumber, is defined as $2\pi/L$, L being wavelength (~50 km) and, therefore, $k = 0.126$, and d, the mean depth of the interface, is ~5 km.

$$42.2(2.8-2.5)1.5 \exp(-0.126 \times 5) = 10 \text{ mGal}$$

Interface (2): $d = 10$ km, $k = 0.126$

$$42.2(3.33-2.8)1.5 \exp(-0.126 \times 10) = 9.5 \text{ mGal}$$

The combined free-air gravity effect is 19.5 mGal, indicating that the short-wavelength acoustic topography of the Coral Sea rift valley is conformable with the Moho topography. Given the accumulating evidence for the existence of an elastic layer supporting both active and inactive rifts[31], it would appear that the 'frozen' ridge topography is most simply explained (though not explicitly modelled) in terms of the thermo-mechanical hysteresis of this elastic layer and is responsible for the observed crustal configuration and free-air gravity anomaly.

Ocean/continent boundaries

The final example relates to the persistent free-air gravity anomaly associated with ocean/continent boundaries, often highlighted by the calculation of an Airy isostatic anomaly, of many passive continental margins. The ocean/continent boundary is characterized by a steep landward gradient, the midpoint of which identifies the position of the boundary as collaborated by magnetic anomalies and reflection seismics[32,38,39]. Some margins also have an associated basement high which appears to be uncompensated[39]. The form of the isostatic anomaly approximates a dipole, centred on the ocean/continent boundary, with the positive and negative components relating to the oceanic and continental sides respectively (Fig. 4*c*). A cause in terms of differential subsidence and flexure between the oceanic and continental crust is considered unlikely because, as noted by Watts and Steckler[40], the mechanical properties of thinned continental and oceanic lithosphere are similar and, therefore, it is not obvious why a flexural deformation between unstretched continental crust and thinned continental/oceanic crust should be centred on the ocean/continent boundary. In the case of the South China Sea (margin age ~30 Myr), the isostatic anomaly[32] has an amplitude of ~30 mGal, ~400 km wavelength, and landward gradient 0.85 mGal km^{-1} (Fig. 4*c*). In contrast, the significantly older Argentinian margin (age ~110 Myr) has an anomaly amplitude of ~60 mGal, 400 km wavelength, and gradient 0.95 mGal km^{-1} (that is, the admittance tends to increase with increasing margin age). The steep gradient demands a relatively shallow source (crustal) while the wavelength and dipole nature of the anomaly suggests that compensation is related to the deformation of the crust. The association of this anomaly with a thermal process across the ocean/continent boundary (the initial continental rifting) again suggests that the ocean/continent boundary anomaly is a product of thermo-mechanical hysteresis.

Conclusions

Long after the cessation of inter- or intraplate thermal activity, the surface of the lithosphere will remain distorted with an amplitude and wavelength dependent on the mechanical properties of the lithosphere and the degree of reheating. This residual topography will remain indefinitely unless reset and hence redistributed by a subsequent thermal event. As the production of residual topography is a hysteresis process, the previous deformation is only replaced by a new deformation—the surface can never return to a stress-free state. Suitable thermal events include intraplate hotspots, formation of ridge topography at spreading centres, and continental (oceanic) rifting leading to the formation of an ocean/continent (ocean/ocean) boundary. Given the ability of the lithosphere to recover mechanically from a superimposed thermal event, the existence of TMH is an undeniable consequence. However, further work will be required to determine its exact importance.

I thank J. K. Weissel, J. F. Dewey, M. H. P. Bott, G. K. Westbrook, and M. S. Steckler for critically reviewing and improving the manuscript, M. D. Broussard and L. G. Karner for special assistance, and especially J. K. Weissel for supplying data relevant to the Cocos-Keeling trend. This work was supported by an Elf-Aquitaine Research Fellowship and the Society of Fellows, University of Durham.

Received 3 April; accepted 7 October 1985.

1. Karner, G. D., Steckler, M. S. & Thorne, J. A. *Nature* **304**, 250-253 (1983).
2. Menard, H. W. & McNutt, M. *J. geophys. Res.* **87**, 8570-8580 (1982).
3. Bodine, J. H., Steckler, M. S. & Watts, A. B. *J. geophys. Res.* **86**, 3695-3707 (1981).
4. Watts, A. B. *J. geophys. Res.* **83**, 5989-6004 (1978).
5. Watts, A. B., Bodine, J. H. & Steckler, M. S. *J. geophys. Res.* **85**, 6369-6376 (1980).
6. Parsons, B. & Sclater, J. G. *J. geophys. Res.* **82**, 803-827 (1977).
7. Crough, S. T. *Tectonophysics* **61**, 321-333 (1979).
8. Crough, S. T. *Bull. geol. Soc. Am.* **95**, 3-8 (1984).
9. Crough, S. T. *Ann. Rev. Earth planet. Sci.* **11**, 165-193 (1983).
10. Crough, S. T. *Geophys. J.R. astr. Soc.* **55**, 451-469 (1978).
11. Detrick, R. S., von Herzen, R. P., Crough, S. T., Epp, D. & Fehn, U. *Nature* **292**, 142-143 (1981).
12. Bonatti, E. & Harrison, C. G. A. *Nature* **263**, 402-404 (1976).
13. Wellman, P. *Tectonophysics* **96**, 225-243 (1983).
14. Smith, A. G. *Nature* **296**, 400-404 (1982).
15. McKenzie, D. *Earth planet. Sci. Lett.* **40**, 25-32 (1978).
16. Royden, L. & Keen, C. E. *Earth planet. Sci. Lett.* **51**, 343-361 (1980).
17. Hellinger, S. J. & Sclater, J. G. *J. geophys. Res.* **88**, 8251-8269 (1983).
18. Banks, R. J., Parker, R. L. & Huestis, S. P. *Geophys. J.R. astr. Soc.* **51**, 431-452 (1977).
19. Karner, G. D. & Watts, A. B. *J. geophys. Res.* **87**, 2923-2948 (1982).
20. Bodine, J. H. *Lamont-Doherty Geological Observatory tech. Rep.* CU-1-80 (1981).
21. Stephenson, R. S. *Geophys. J.R. astr. Soc.* **77**, 385-414 (1984).
22. Stephenson, R. S. & Lambeck, K. *Geophys. J.R. astr. Soc.* **82**, 31-56 (1985).
23. Beaumont, C. *Geophys. J.R. astr. Soc.* **65**, 291-329 (1981).
24. Beaumont, C. *Geophys. J.R. astr. Soc.* **55**, 471-497 (1978).
25. Lambeck, K. *Geophys. J.R. astr. Soc.* **74**, 843-886 (1983).
26. Lambeck, K., McQueen, H., Stephenson, R. & Denham, D. *Annls Geophys.* **2**, 723-741 (1984).
27. McNutt, M. K. *J. geophys. Res.* **89**, 11180-11194 (1984).
28. Pryce, C. thesis, Univ. Durham (1984).
29. Liu, C-S., Sandwell, D. T. & Curray, J. R. *J. geophys. Res.* **87**, 7673-7686 (1982).
30. Weissel, J. K. & Watts, A. B. *J. geophys. Res* **84**, 4572-4582 (1979).
31. Watts, A. B. *Geodynamic Ser. 8* (ed. Palmason, G.) 99-106 (American Geophysics Union, Washington, DC, 1982).
32. Taylor, B. & Hayes, D. E. *Geophys. Monogr.* **27**, Pt 2, 23-56 (1983).
33. Cameron, P. J. *et al. 18th General Assembly of the International Union of Geodesy and Geophysics*, Canberra, Abstr. 5-6 (1979).
34. Cochran, J. R. *J. geophys. Res.* **84**, 4713-4729 (1979).
35. McNutt, M. *J. Geophys. Res.* **84**, 7589-7598 (1979).
36. Stoffa, P. L., Buhl, P., Herron, T. J., Khan, T. K. & Ludwig, W. J. *Mar. Geol.* **35**, 83-97 (1980).
37. Madsen, J. A., Forsyth, D. W. & Detrick, R. S. *J. geophys. Res.* **89**, 9997-10015 (1984).
38. Rabinowitz, P. D. & LaBrecque, J. L. *Earth planet. Sci. Lett.* **35**, 145-150 (1977).
39. Rabinowitz, P. D. & LaBrecque, J. *J. geophys. Res.* **84**, 5973-6002 (1979).
40. Watts, A. B. & Steckler, M. S. in *Deep Drilling Results in the Atlantic Ocean: Continental Margins and Palaeoenvironment* (eds Talwani, M., Hays, W. & Ryan, W. B.) 218-234 (Maurice Ewing Ser. 3, American Geophysics Union, Washington, DC, 1979).
41. Minister, J. B. & Jordan, T. H. *J. geophys. Res.* **83**, 5331-5354 (1978).
42. Rabinowitz, P. D. in *The Geology of Continental Margins* (eds Burke, C. A. & Drake, C. L.) 67-84 (Springer, Berlin, 1974).